Journal of Alloys and Compounds 509 (2011) 3057–3064

Contents lists available at ScienceDirect

Journal of Alloys and Compounds

journal homepage: www.elsevier.com/locate/jallcom

Thermodynamic modeling of the Au–Sb–Si ternary system

J. Wang[a,d,*], Y.J. Liu[b], L.B. Liu[c], H.Y. Zhou[a], Z.P. Jin[c]

[a] School of Materials Science and Engineering, Guilin University of Electronic Technology, Guilin, Guangxi 541004, PR China
[b] Western Transportation Institute, Montana State University, Bozeman, MT 59715, USA
[c] School of Materials Science and Engineering, Central South University, Changsha, Hunan 410083, PR China
[d] Swiss Federal Laboratories for Materials Science and Technology, Laboratory for Joining and Interface Technology, Überlandstrasse 129, Dübendorf, Zürich CH-8600, Switzerland

ARTICLE INFO

Article history:
Received 23 August 2010
Received in revised form
25 November 2010
Accepted 30 November 2010
Available online 7 December 2010

Keywords:
Au-based alloys
Phase diagram
CALPHAD
Au–Sb–Si ternary system

ABSTRACT

Thermodynamic optimization of the Au–Sb binary system was updated as well as the Si–Sb binary system was assessed thermodynamically using the CALPHAD method based on the critical review of the available experimental information from the published literature. The solution phases including liquid, fcc_A1(Au), diamond_A4(Si) and rhombohedral_A7(Sb), are modeled as substitutional solutions and their excess Gibbs energies are expressed by a Redlich–Kister polynomial. The solubility of Si in the intermetallic compound $AuSb_2$ is not taken into account because of the lack of experimental information. Combined with previous assessment of the Au–Si binary system, thermodynamic modeling of the Au–Sb–Si ternary system was performed to reproduce well the measured phase equilibria. The liquidus projection and several vertical sections of this ternary system were calculated, which are in reasonable agreement with the reported experimental data.

1. Introduction

High-Pb solders (e.g. Pb–5 wt.% Sn) as high-temperature solders have been widely used in advanced electronic packaging of the electronic and automotive industries. However, Pb is harmful to both the environment and human health. Therefore, the development of high-temperature Pb-free solders to replace the conventional high-Pb solders has become an important issue now [1–3]. Many alloys such as Zn-based alloys (Zn–Al, Zn–Sn) [4,5], Bi-based alloys (Bi–Ag) [6], Sn–Sb alloys [7] and Au-based alloys (Au–Sn, Au–Si, Au–Sb, Au–Ge) [8–11] have been proposed as alternative high-temperature Pb-free solders [4–11]. Despite their high price, Au-based alloys as high temperature solders are quite useful for bonding applications in microelectronic and optoelectronic packages due to their excellent properties (e.g. superior resistance to corrosion, high electrical and thermal conductivity, excellent mechanical strength) [8–11]. Especially, Au–20 wt.% Sn eutectic alloy is attractive in high power electronic and optoelectronic devices because of its superior resistance to corrosion and high electrical and thermal conductivity as well as high mechanical strength [8–11]. To reduce the costs of Au-based solders, alloying elements such as Ag, Al, Bi, Cu, Ga, Ge, In, Sb, Si, Zn, etc., may be added to replace a part of the Au. In order to understand better the role of alloying elements and to design novel Au-based solders, knowledge of the precise phase diagrams and reliable thermodynamic properties of the Au-based alloy systems is indispensable. Recently, thermodynamic descriptions of many binary and ternary systems including Au–Pb, Au–Al, Au–In, Au–Zn binary systems and Au–Ag–Si, Au–Ag–Sn, Au–Bi–Sb, Au–Ge–Sn, Au–Ge–Sb, Au–Ge–Si, Au–Ag–Pb, Au–In–Sn, Au–In–Sb, Au–Si–Sn and Au–Co–Sn ternary systems have been developed by Wang, Liu and Jin [12–26] using the CALPHAD method [27,28]. Thermodynamic database of the corresponding binary and ternary systems has been established on the basis of their assessments.

As a contribution to establish a consistent and available thermodynamic database of the Au-based multicomponent alloys, the purpose of the present work is to evaluate firstly the experimental phase diagram and thermodynamic data of the Au–Sb and Sb–Si binary systems and to obtain a consistent and reliable thermodynamic description of the Au–Sb–Si ternary system in combination with the previous assessment of the Au–Si binary system using the CALPHAD method [27,28] and Thermo-calc® software package [29].

2. Binary systems

2.1. The Au–Si binary system

The Au–Si binary system has been optimized thermodynamically by Meng et al. [25] in the assessment of the Au–Si–Sn ternary system. Good agreements are achieved between the calculated

* Corresponding author at: EMPA, Swiss Federal Laboratories for Materials Science and Technology, Laboratory for Joining and Interface Technology, Überlandstrasse 129, Dübendorf, Zürich CH-8600, Switzerland.
Tel.: +41 44 823 4250; fax: +41 44 823 4011.
E-mail addresses: jiang.wang@empa.ch, wangjiang158@gmail.com (J. Wang).

0925-8388/$ – see front matter © 2010 Elsevier B.V. All rights reserved.
doi:10.1016/j.jallcom.2010.11.199

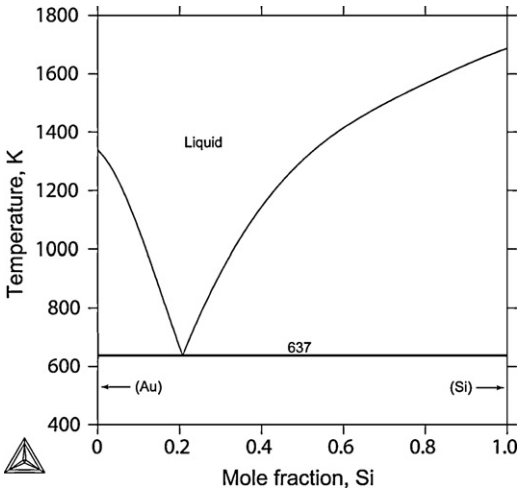

Fig. 1. Phase diagram of the Au–Si binary system calculated by Meng et al. [25].

phase diagrams as well as thermodynamic properties and the reported experimental information. The thermodynamic parameters formulating the Gibbs energies of various phases in the Au–Si binary system obtained by Meng et al. [25] were employed directly in the present work. The calculated phase diagram of the Au–Si binary system is shown in Fig. 1.

2.2. The Au–Sb binary system

The Au–Sb binary system was reviewed by Okmoto and Massalski [30] and then was optimized by Chevalier [31]. Afterwards, Kim et al. [32] re-optimized the Au–Sb binary system with the assumption that the enthalpy of mixing of the liquid phase is independent of temperature. At the same time, Liu et al. [20] assessed the Au–Sb binary system based on the critical review of the reported experimental information, considering the temperature dependence of mixing enthalpy of the liquid phase. The different descriptions of the liquid phase were employed in these two assessments [20,32]. Although the optimization of Kim et al. [32] can reproduce well the reported experimental information, too many thermodynamic parameters were used to describe the liquid phase. On the other hand, the temperatures of the invariant reactions assessed by Liu et al. [20] deviate slightly from the experimental values. Therefore, thermodynamic optimization of the Au–Sb binary system was updated in the present work.

2.3. The Sb–Si binary system

The available phase equilibria data of the Sb–Si binary system in the published literature was reviewed critically by Olesinki and Abbaschian [33]. The primary calculation of this binary system was also carried out according to the phase diagram data. However, the lattice stabilities of the elements Sb and Si used in Ref. [33] are different from those proposed by Dinsdale [34]. In order to achieve the compatibility of thermodynamic databases in the multi-component systems, thermodynamic parameters of various phases in the Sb–Si binary system were assessed in the present work.

3. Experimental information

3.1. The Au–Sb binary system

In the Au–Sb binary system, there are four condensed phases including liquid, fcc_A1(Au), rhombohedral_A7(Sb) and intermetallic compound $AuSb_2$ with Fe_2S-type structure. $AuSb_2$ was reported to form through a peritectic reaction, $L + (Sb) \leftrightarrow AuSb_2$, at about 723–733 K measured by Vogel [35] using thermal anal-

Table 1
Invariant reactions in the Au–Sb–Si ternary system.

System	Reaction	Type	T (K)	Composition		Reference
				x^L_{Sb}	x^L_{Si}	
Sb–Si system	$L \leftrightarrow (Sb) + (Si)$	e_1	903	0.999	0.001	[51]
			903	0.997	0.003	[52]
			903	0.997	0.003	[33]
			903	0.997	0.003	This work
Au–Si system	$L \leftrightarrow (Au) + (Si)$	e_2	637	–	0.207	[25]
Au–Sb system	$L + (Sb) \leftrightarrow AuSb_2$	p_1	723–733	~0.66	–	[35]
			725–736	~0.66	–	[36]
			733	–	–	[37]
			733	–	–	[38]
			740	–	–	[39]
			732	0.670	–	[40]
			733	0.666	–	[30]
			734	0.663	–	[31]
			733	0.655	–	[32]
			740	0.655	–	[20]
			732	0.653	–	This work
	$L \leftrightarrow (Au) + AuSb_2$	e_3	630–634	–	–	[35]
			624–631	–	–	[36]
			633	–	–	[38]
			634	–	–	[39]
			630	–	–	[41]
			631	0.360	–	[40]
			633	0.355	–	[30]
			630	0.349	–	[31]
			633	0.362	–	[32]
			626	0.366	–	[20]
			630	0.369	–	This work
Au–Sb–Si system	$L + (Sb) \leftrightarrow (Si) + AuSb_2$	U	730	–	–	[60]
			732	0.649	0.002	This work
	$L \leftrightarrow (Au) + (Si) + AuSb_2$	E	605	0.200	0.100	[60]
			604	0.125	0.135	[62]
			608	0.133	0.135	This work

Table 2
Thermodynamic parameters of the Au–Sb–Si ternary system.

Phase	Thermodynamic parameter[a]	Reference
Liquid (Au, Sb, Si)	${}^{(0)}L_{Au,Sb} = -10348.21 - 16.183T$	This work
	${}^{(1)}L_{Au,Sb} = -2697.56 - 6.915T$	
	${}^{(0)}L_{Au,Si} = -24103.3028 - 15.13883T$	
	${}^{(1)}L_{Au,Si} = -29375.2777 + 1.1065T$	[25]
	${}^{(2)}L_{Au,Si} = -13032.2412$	
	${}^{(0)}L_{Sb,Si} = +15463.82+4.805T$	This work
	${}^{(0)}L_{Au,Sb,Si} = +27522$	
	${}^{(1)}L_{Au,Sb,Si} = +40647$	This work
	${}^{(2)}L_{Au,Sb,Si} = -32270$	
fcc_A1 (Au, Sb, Si)	${}^{(0)}L_{Au,Sb} = +24512.70 + 25T$	This work
	${}^{(0)}L_{Au,Si} = +2000$	[25]
Rhombohedral_A7 (Sb)	${}^{0}G_{Sb}^{Rho.}$ cited from SGTE database	[34]
	${}^{0}G_{Sb}^{Dia.} - {}^{0}G_{Sb}^{Rho.} = +4184$	[17]
Diamond_A4 (Au, Sb, Si)	${}^{(0)}L_{Au,Si} = +40000$	[25]
	${}^{(0)}L_{Sb,Si} = +67795.81$	This work
$AuSb_2$ $(Au)_{0.3333}(Sb)_{0.6667}$	$G_m^{AuSb_2} = 0.3333{}^{0}G_{Au}^{fcc} + 0.6667{}^{0}G_{Sb}^{Rho.} - 5549.56 + 5.440T - 0.470T\ln T$	This work

[a] *Note*: Gibbs energies are expressed in J/mol. The all lattice stabilities of Au, Sb and Si are given by Dinsdale [34].

ysis and microscopy. This peritectic reaction was determined by Grigorjew [36] and Evans and Prince [37] by thermal analysis, Gaither and Blachnik [38] through X-ray diffraction (XRD), Wallbrecht et al. [39] and Zoro et al. [40] using differential scanning calorimetry. The eutectic reaction, $L \leftrightarrow (Au) + AuSb_2$, was measured by Vogel [35], Grigorjew [36], Gaither and Blachnik [38], Wallbrecht et al. [39], Zoro et al. [40], Hayer and Castanet [41]. The experimental results of the invariant reactions mentioned above as summarized in Table 1 are generally consistent with each other and were accepted in the present work.

Phase boundaries of the liquid phase were measured by Vogel [35], Grigorjew [36] as well as Evans and Prince [37] using thermal analysis and microscopic examination. Hayer and Castanet [41] determined the liquidus by means of thermal analysis and calorimetry method. The experimental results measured by Vogel [35], Grigorjew [36], Evans and Prince [37], Hayer and Castanet [41] agree well with each other in the Sb-rich part, although the experiment values [35] show slight deviation from the experimental results [37,41] in the Au-rich part. Considering the good agreement between the experimental values from both thermal analysis and calorimetry method, the experimental results [37,41] are much more reliable and were thus given larger weights than the other experimental values [35–36] during the optimization.

The solubility of Sb in the fcc_A1(Au) phase was determined by Owen and Roberts [42] through lattice parameter measurements. Experimental data on the solubility of Au in rhombohedral_A7(Sb) could not be found in the published literature. Therefore, the solubility of Sb in fcc_A1(Au) was taken into account, while the solubility of Au in rhombohedral_A7(Sb) was neglected in the present optimization.

The enthalpies of mixing of the liquid Au–Sb alloys referred to liquid Au and liquid Sb were measured by Hayer and Castanet [41] at different temperatures (906–1028 K) and Anres et al. [43] at 916 K using calorimetry method. The experimental data obtained by Hayer and Castanet [41] and Anres et al. [43] are compatible with each other in the Sb-rich part, but are scattered in the composition range of 20–60 at.% Sb. The temperature dependence of mixing enthalpies of liquid alloys is not obvious due to the scattered experimental data at different temperatures and thus was not taken into account in the present optimization.

Activities of Sb in the liquid Au–Sb alloys were determined by Kameda et al. [44] at 973 K and 1073 K through the electromotive force (EMF) method as well as Hino et al. [45] at 1273 K, 1373 K and 1473 K by means of vapour pressure measurements. The experimental information [44,45] was used during the present optimization.

The enthalpies of formation of intermetallic compound $AuSb_2$ were measured by Hayer and Castanet [41], Jena and Bever [46], Weibke and Schrag [47] at 298 K, Biltz [48] at 363 K and Kleppa [49] at 723 K. The reported experimental data [46,47] at 298 K differ much from the determined value later by Hayer and Castanet [41]. Experimental value [41] could be more reliable and thus was used in the present optimization, while the other experimental data [46–49] were neglected. According to these experimental values [41,46–49], the temperature dependence of formation enthalpy of $AuSb_2$ is assumed. In addition, the enthalpy contents $(H_T - H_{298})$ of $AuSb_2$ and the alloy with 36 at.% Sb (eutectic composition) were measured by Anres et al. [43] (298–963 K) and Yassin et al. [50] (298–846 K) using calorimetry, respectively. The experimental results [43,50] were also considered in the present optimization.

3.2. The Sb–Si binary system

The Sb–Si binary system is a simple eutectic system. In 1907, Williams [51] investigated firstly the liquidus of the Si-rich part using thermal analysis. Several liquidus points were determined by Thurmond and Kowalchik [52] and Girault [53] using a weighing technique with high purity of the materials and the temperature measurements are accurate within the experimental error (±2 K). Two liquidus points were also measured by Malmeja et al. [54] using differential thermal analysis (DTA) and the estimated temperature error of these measurements is about ±3 K. Although Si contained almost 2% impurities (mainly Fe and Al) in the measurements of Ref. [51] could affect the thermal analysis results, the experimental results [51] are still consistent with the reported experimental data [52–54]. On the other hand, the temperature and composition of the eutectic reaction in the Sb–Si binary system were estimated by Williams [51], Thurmond and Kowalchik [52] from their experimental results and were also reviewed by Olesinki and Abbaschian [33] as given in Table 1. The reported temperature and composition for this eutectic reaction are very close to the melting point of Sb and pure Sb, respectively. The experimental information mentioned above [51–54] was taken into account in the present optimization.

Experimental information concerning the solubility of Si in rhombohedral_A7(Sb) could not be found in the published literature. Although a very small solubility of Sb in diamond_A4(Si) was reported by Fuller and Ditzenberger [55], Rohan et al. [56], Trumbore [57] and Nobili et al. [58], the solubility of terminal solid solutions in the Sb–Si binary system was not taken into account in the present optimization.

According to the thorough review of the published literature, no thermodynamic properties of the Sb–Si binary system (such as mixing enthalpy, activity etc.) have been reported up to now.

3.3. The Au–Sb–Si ternary system

No thermodynamic properties of the Au–Sb–Si ternary system have been reported in terms of the published literature. Gubenko and Kiparisova [59] as well as Legendre and Hancheng [60] investigated experimentally this ternary system. According to the experimental results [59,60], no stable ternary compound was found in this ternary system. Prince et al. [61] reviewed this ternary system when compiled phase diagrams of Au-based alloys.

Gubenko and Kiparisova [59] determined the liquidus in the region of primary solidification of Si for three vertical sections close to the Au–Si binary side of the Au–Sb–Si ternary system (Au–0.16 at.% Sb–Si, Au–1.13 at.% Sb–Si and Au–1.61 at.% Sb–Si) in the temperature range from 823 K to 1073 K. However, after analyzed and checked carefully their experimental results [59], Prince et al. [61] pointed out that the measured liquidus is not reliable because the formed liquid phase of ternary Au–Sb–Si alloys is assumed to be saturated with Si at each temperature. Legendre and Hancheng [60] investigated experimentally phase relations of this ternary system through differential thermal analysis and differential scanning calorimetry. Five vertical sections, at 10 at.% Si, 10 at.% Sb, 30 at.% Sb, 50 at.% Sb, 80 at.% Au, have been measured. Experimental results obtained by Legendre and Hancheng [60] show that the Au–Sb–Si ternary system contains two invariant reactions: a transition reaction (U) at 730 K, L + rhombohedral_A7(Sb) ↔ diamond_A4(Si) + $AuSb_2$ and a eutectic reaction (E) at 605 K, $L \leftrightarrow$ fcc_A1(Au) + diamond_A4(Si) + $AuSb_2$. The composition of the liquid phase for the eutectic reaction (E) was determined, while those of the terminal solid solutions including fcc_A1(Au), diamond_A4(Ge) and rhombohedral_A7(Sb) as well as the composition of the transition reaction (U) were not measured. On the basis of the experimental results [60], the liquidus projection of this ternary system was constructed. Recently, Humpston and Sangha [62] redetermined the composition and temperature of the eutectic reaction (E) in the Au–Sb–Si ternary system through metallographic examination and thermal analysis. The obtained temperature of the eutectic reaction (604 K) is in good agreement with the experimental value (605 K) by Legendre and Hancheng [60], while the liquid composition of the eutectic reaction (12.5 at.% Sb, 13.5 at.% Si) differ obviously from the previous experimental results (20 at.% Sb, 10 at.% Si) [60].

4. Thermodynamic models

4.1. Pure elements

The stable forms of the pure elements at 298.15 K and 1 bar are chosen as the reference states of the system. The Gibbs energy for the element i in ϕ status is given as:

$$^{0}G_i^{\phi}(T) = G_i^{\phi}(T) - H_i^{SER} = a + b\cdot T + c\cdot T\ln T + d\cdot T^2 + e\cdot T^3 + f\cdot T^{-1} + g\cdot T^7 + h\cdot T^{-9} \quad (1)$$

where H_i^{SER} is the enthalpy of the element i in its standard reference state (SER) at 298.15 K and 1 bar; T is the absolute temperature in K; $G_i^{\phi}(T)$ is the Gibbs energy of the element i with structure ϕ; $^{0}G_i^{\phi}(T)$ is the molar Gibbs energy of the element i with the structure of ϕ referred to the enthalpy of its stable state at 298.15 K and 1 bar. In the present work, the Gibbs energies of the elements Au, Sb and Si, $^{0}G_{Au}^{\phi}(T)$, $^{0}G_{Sb}^{\phi}(T)$ and $^{0}G_{Si}^{\phi}(T)$ are taken from the SGTE (Scientific Group Thermodata Europe) database compiled by Dinsdale [34].

4.2. Solution phases

The substitutional solution model is employed to describe the solution phases including Liquid, fcc_A1(Au), rhombohedral_A7(Sb) and diamond_A4(Si), respectively. The molar Gibbs energy of the solution phase ϕ (ϕ = Liquid, fcc_A1, rhombohedral_A7 and diamond_A4) can be expressed as:

$$G_m^{\phi} = \sum x_i\,^{0}G_i^{\phi} + RT\sum x_i\ln(x_i) + {}^{E}G_m^{\phi} \quad (2)$$

where $^{0}G_i^{\phi}$ is the molar Gibbs energy of the element i (i = Au, Sb, Si) with the structure ϕ, x_i the mole fraction of component i, R gas constant, T temperature in K, $^{E}G_m^{\phi}$ the excess Gibbs energy. The excess Gibbs energy of phase ϕ can be expressed by the Redlich–Kister–Muggianu polynomial [63,64] as:

$$^{E}G_m^{\phi} = x_{Au}x_{Sb}\sum_{j=0}^{n}{}^{(j)}L_{Au,Sb}^{\phi}(x_{Au}-x_{Sb})^j + x_{Au}x_{Si}\sum_{j=0}^{n}{}^{(j)}L_{Au,Si}^{\phi}(x_{Au}-x_{Si})^j + x_{Sb}x_{Si}\sum_{j=0}^{n}{}^{(j)}L_{Sb,Si}^{\phi}(x_{Sb}-x_{Si})^j + x_{Au}x_{Sb}x_{Si}L_{Au,Sb,Si}^{\phi} \quad (3)$$

with

$$^{(j)}L_{Au,Sb}^{\phi} = A_j + B_jT \quad (4)$$

$$^{(j)}L_{Sb,Si}^{\phi} = C_j + D_jT \quad (5)$$

$$L_{Au,Sb,Si}^{\phi} = x_{Au}{}^{(0)}L_{Au,Sb,Si} + x_{Sb}{}^{(1)}L_{Au,Sb,Si} + x_{Si}{}^{(2)}L_{Au,Sb,Si} \quad (6)$$

where A_j, B_j, C_j and D_j are parameters to be optimized in the present work. $^{(j)}L_{Au,Si}^{\phi}$ is binary interaction parameter, which is taken directly from the Au–Si binary systems assessed by Meng et al. [25]. The ternary interactive parameters $^{(j)}L_{Au,Sb,Si}$ are parameters to be evaluated in the present work.

4.3. Intermetallic compound

In the Au–Sb binary system, $AuSb_2$ is treated as a stoichiometric compound because of the narrow homogeneity range. Since the heat contents and enthalpies of formation of $AuSb_2$ at different temperatures were determined [41,43], the molar Gibbs energy of $AuSb_2$ is expressed as follows:

$$G_m^{AuSb_2} = 0.3333\,^{0}G_{Au}^{fcc} + 0.6667\,^{0}G_{Sb}^{Rho\cdot} + E_1 + E_2T + E_3T\ln T \quad (7)$$

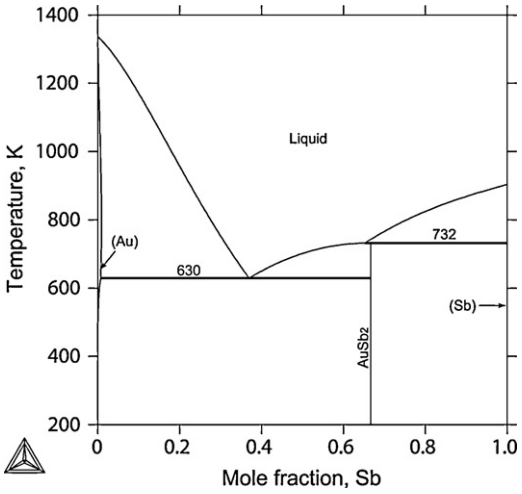

Fig. 2. Phase diagram of the Au–Sb binary system calculated in the present work.

where E_1, E_2 and E_3 are parameters to be optimized in the present work.

In the Au–Sb–Si ternary system, the solubility of Si in $AuSb_2$ was not considered due to the lack of the available experimental information. Thus the Gibbs energy of the intermetallic compound $AuSb_2$ was taken directly from the Au–Sb binary system in the present work during the optimization and calculation of this ternary system.

5. Results and discussion

Using the lattice stabilities of the elements Au, Sb and Si compiled by Dinsdale [34], the model parameters for various phases in the Au–Sb–Si ternary system was optimized using the PARROT module in the Thermo-calc® software package developed by Sundman et al. [29]. This module works by minimizing the square sum of the differences between the experimental data and calculated values. In the optimization procedure, each set of experimental data was given a certain weight. The weights were changed systematically during the optimization until most of experimental data was accounted for within the claimed uncertainty limits.

Thermodynamic parameters for all condensed phases in the Au–Sb–Si system used and obtained eventually in the present work are summarized in Table 2. Table 1 shows the invariant reactions for the Sb–Si, Au–Sb, Au–Si binary systems and the Au–Sb–Si ternary system, respectively. Reasonable agreement is achieved between the calculated results and the experimental data.

5.1. The Au–Sb binary system

Fig. 2 is the calculated phase diagram of the Au–Sb binary system. The comparison of the calculated phase diagram with the experimental data measured by Vogel [35], Grigorjew [36], Evans and Prince [37], Hayer and Castanet [41] as well as Owen and Roberts [42] is shown in Fig. 3. As can be seen, the calculated liquidus is in good agreement with the experimental data [35–37,41,42], especially in the Sb-rich part. The calculated solubility of Sb in fcc(Au) is also consistent with the experimental data [42]. The calculated temperatures and compositions of the invariant reactions are given in Table 1 with the experimental values [35–41] and the previously assessed values [20,30–32]. The calculated temperatures of the eutectic reaction (e_3) and peritectic reaction (p_1) are 630 K and 732 K in the present work, respectively, which agree better with the experimental values [35–41] than the previous assessment [20] (626 K and 740 K).

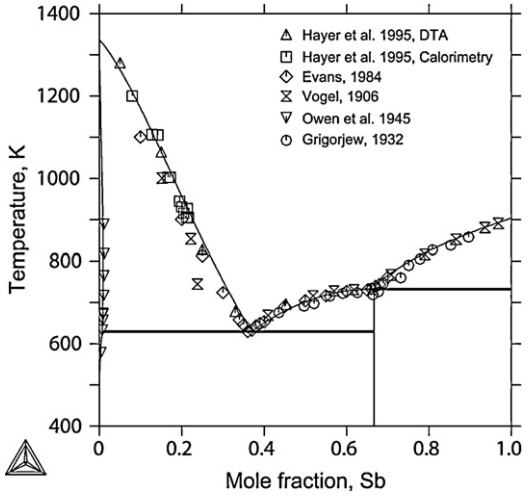

Fig. 3. Calculated phase diagram of the Au–Sb binary system with the experimental data [35–37,41,42] in the present work.

The comparison of the enthalpies of mixing of the liquid Au–Sb alloys between the calculated and experimental values at 938 K is presented in Fig. 4. It can be seen that the calculated mixing enthalpies agree well with the experimental data determined by Hayer and Castanet [41] in the Sb-rich part, but show some deviation from the experimental data measured Anres et al. [43] in the Au-rich part. The similar cases are also shown in the previous assessments [20,32]. Considering the scattered data in the Au-rich part and experimental error, the present calculation is still reasonable.

Fig. 5 shows the comparisons between the calculated activities of Sb in the liquid Au–Sb alloys with the experimental data [44,45] at different temperatures (973 K, 1073 K, 1273 K, 1373 K and 1473 K). The calculated results show their compatibility with the experimental data measured by Kameda et al. [44], but deviate slightly from the experimental values reported by Hino et al. [45]. The similar cases also show in the previous assessments [20,32]. However, they are still reasonable and acceptable because the activity of a component determined by the EMF method is much more reliable and within a smaller experimental error than that determined by vapour pressure method. Moreover, the calculated activities of Sb in liquid Au–Sb alloys in the present work

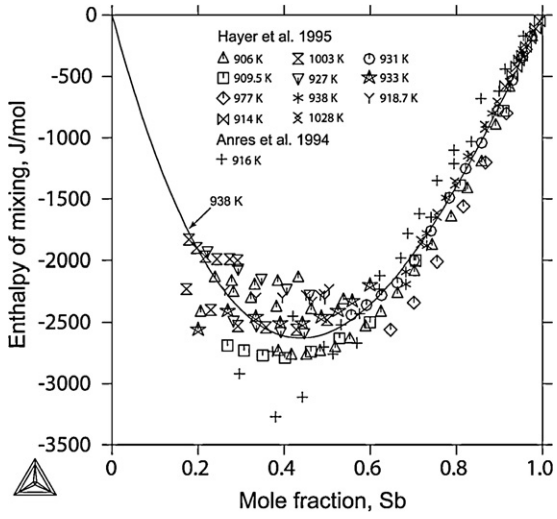

Fig. 4. Calculated enthalpy of mixing of the liquid Au–Sb binary alloys in comparison with the experimental data [41,43] at 938 K (Ref. states: liquid Au and Sb).

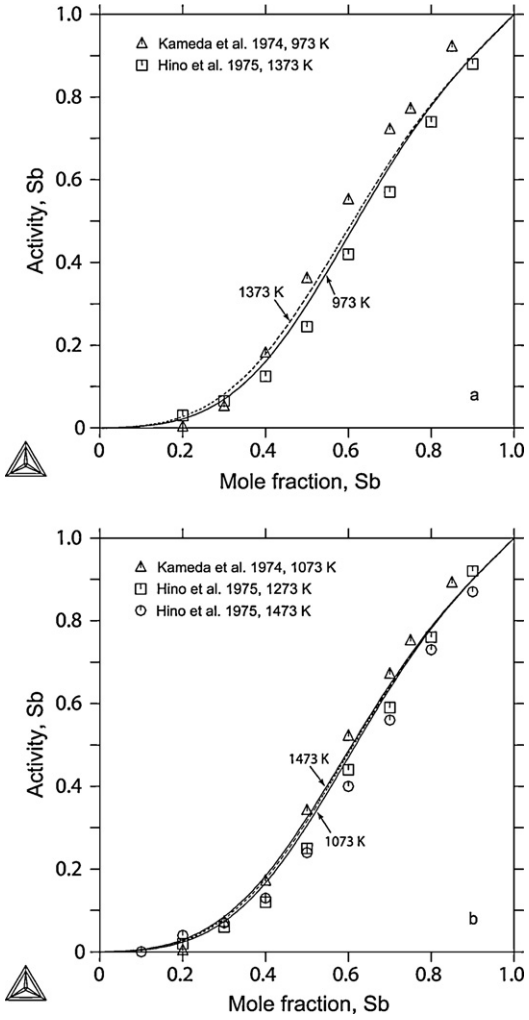

Fig. 5. Calculated activities of Sb in liquid Au–Sb alloys with the experimental data [44,45] (Ref. state: liquid Sb). (a) 973 K and 1373 K and(b) 1073 K, 1273 and 1473 K.

become closer to its molar fraction with increasing temperature, which obeys the rule that liquid phase should become closer to ideal solution at higher temperature. However, the experimental data reported by Kameda et al. [44] and Hino et al. [45] are not in agreement with this tendency in the Sb-rich part, which indicates that there are larger experimental error in these two measurements [44,45].

The enthalpy of formation of $AuSb_2$ referred to fcc_A1(Au) and rhombohedral_A7(Sb) at 298 K is calculated to be −5409.55 J/mol, which agrees well with the experimental values measured by Hayer and Castanet [41] (−5400 ± 600 J/mol) as well as the assessed values by Liu et al. [20] (−4962 J/mol) and Kim et al. [32] (−5500 J/mol).

Fig. 6 is the calculated enthalpy contents of $AuSb_2$ and the alloy with 36 at.% Sb in comparison with the experimental data measured by Anres et al. [43] and Yassin and Castanet [50]. It can be seen that the calculated enthalpy content of $AuSb_2$ agrees well with the experimental data [43]. However, the calculated enthalpy content of the alloy with 36 at.% Sb deviates from the experimental data [50] at low temperature. The reason for the deviation could result from the uncertainty of the experimental data [50]. As a rule, if the temperature decreases to 298 K, the enthalpy content should become to be zero. As can be seen in Fig. 6, the large uncertainty has to be given to the experimental data [50] in order to get a zero value of the enthalpy content when the temperature is extrapolated to 298 K, while the uncertainty of the measured enthalpy content

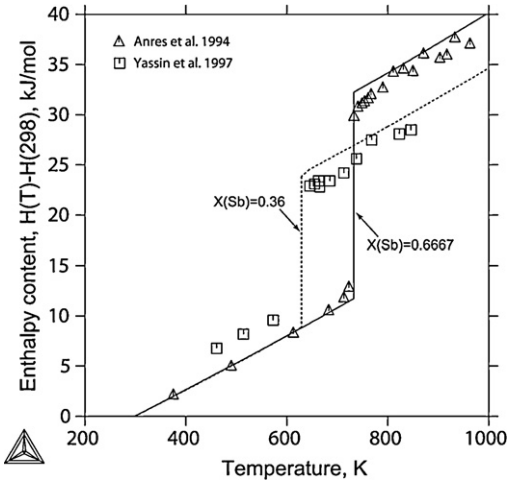

Fig. 6. Calculated enthalpy contents for $AuSb_2$ and the alloy with 36 at.% Sb (eutectic composition) in comparison with the experimental data [43,50].

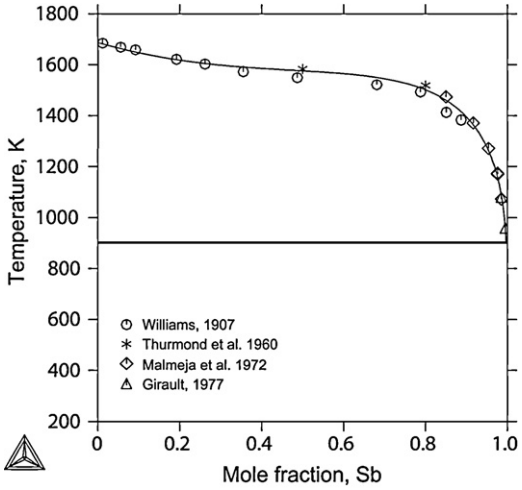

Fig. 8. Calculated phase diagram of the Sb–Si binary system compared with experimental data [51–54] in the present work.

for $AuSb_2$ may be small [43]. Therefore, the present calculation is more reasonable than the experimental data.

5.2. The Sb–Si binary system

The calculated phase diagram of the Sb–Si binary system is shown in Fig. 7, and the comparison of the calculated phase diagram with the experimental data by Williams [51], Thurmond and Kowalchik [52], Girault [53] and Malmeja et al. [54] is presented in Fig. 8. The calculated liquidus is in excellent agreement with most experimental data. In addition, although the solubility of Sb in diamond_A4(Si) is not considered during the optimization, the calculated phase boundary of diamond_A4(Si) is also consistent with the experimental data in Refs.[55–58] as given in Fig. 9. In combination with Table 1, the calculated temperature and composition of the eutectic reaction is in good agreement with the experimental values [33,51,52].

In Section 3 mentioned above, thermodynamic properties of the liquid Sb–Si alloys was not reported in the published literature up to now. As can be seen in Figs. 7 and 8, both the calculated phase diagram of the Sb–Si binary system and the experimental data show smooth liquidus, resulting in a possible metastable liquid miscibility gap, which are corresponding with the positive enthalpies of mixing of the liquid Sb–Si alloys and the activities of Sb and Si are positive deviation from the Raoult's law. The present authors suggest the further experimental investigations to verify these present predictions.

5.3. The Au–Sb–Si ternary system

Combined the present optimizations of the Au–Sb and Sb–Si binary system with the previous assessment of the Au–Si binary systems, the Au–Sb–Si ternary system was further optimized based on available experimental data. The invariant reactions of this ternary system are calculated as shown in Table 1. The liquidus projection and several vertical sections of this ternary system are also calculated and compared with the experimental data in Figs. 10–13.

The invariant reactions (U and E) in the Au–Sb–Si ternary system are associated with the liquid phase as given in Fig. 10 and Table 1. The calculated temperatures of the invariant reactions agree well with the experimental data measured by Legendre and Hancheng [60] and Humpston and Sangha [62], while the calculated compositions of the liquid phase for the eutectic reaction (E) is slight deviation from the experimental data [60], but agree well with the experimental results [62]. In Fig. 10(b), the calculated liquidus projection of the Au-rich part is compared with the experimental results of the primary solidification fields including fcc(Au),

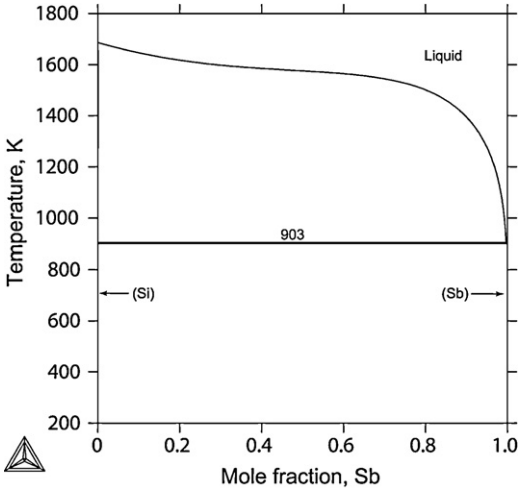

Fig. 7. Calculated phase diagram of the Sb–Si binary system in the present work.

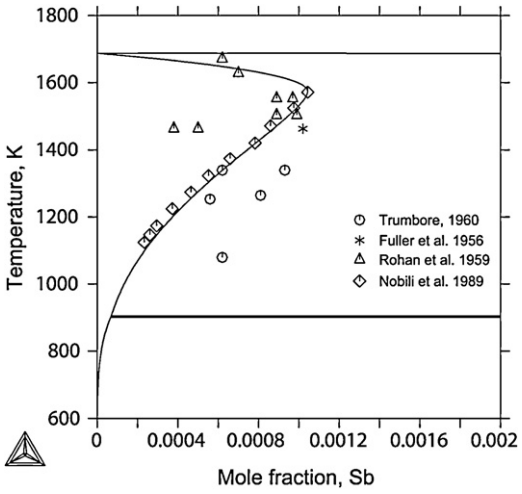

Fig. 9. Calculated phase diagram of the Sb–Si binary system compared with experimental data [55–58] in the Si-rich side in the present work.

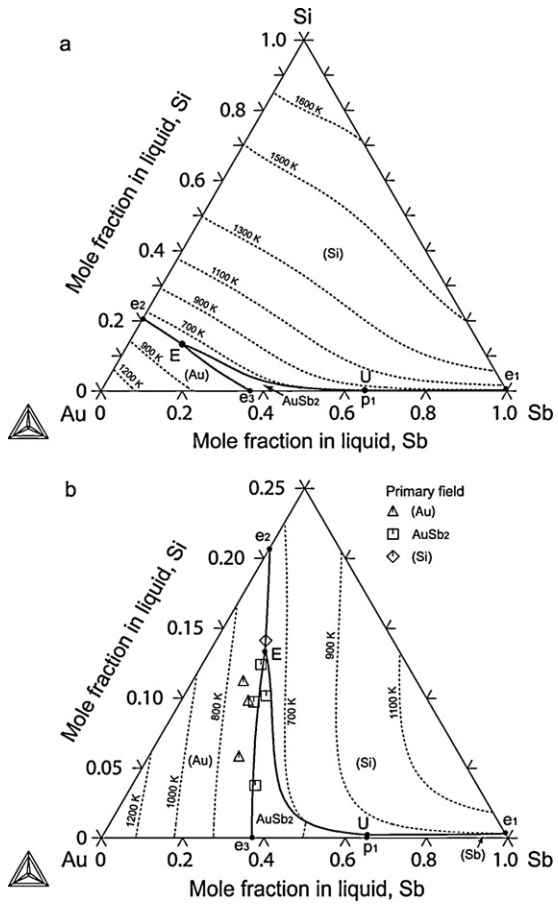

Fig. 10. Calculated liquidus projection of the Au–Sb–Si ternary system in the present work. (a) Overview and (b) Au-rich part with the experimental results of the primary phases [62].

dimond(Si) and $AuSb_2$. As can be seen, the calculated results are consistent with the experimental results [62].

Figs. 11–13 present the calculated vertical sections at 80 at.% Au, 10 at.% Sb, 30 at.% Sb, 50 at.% Sb and 10 at.% Si with the experimental data [60], respectively. It can be seen that the calculated phase relations and phase boundaries are in good agreement with the experimental data [60]. In Figs. 11 and 13, the calculated liquidus

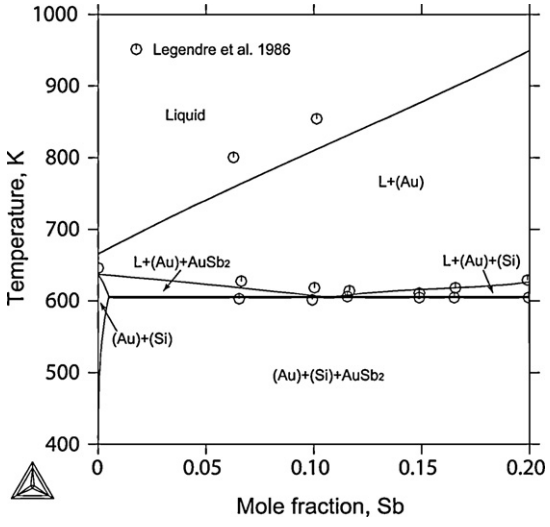

Fig. 11. Calculated vertical section at 80 at.% Au with the experimental data [60].

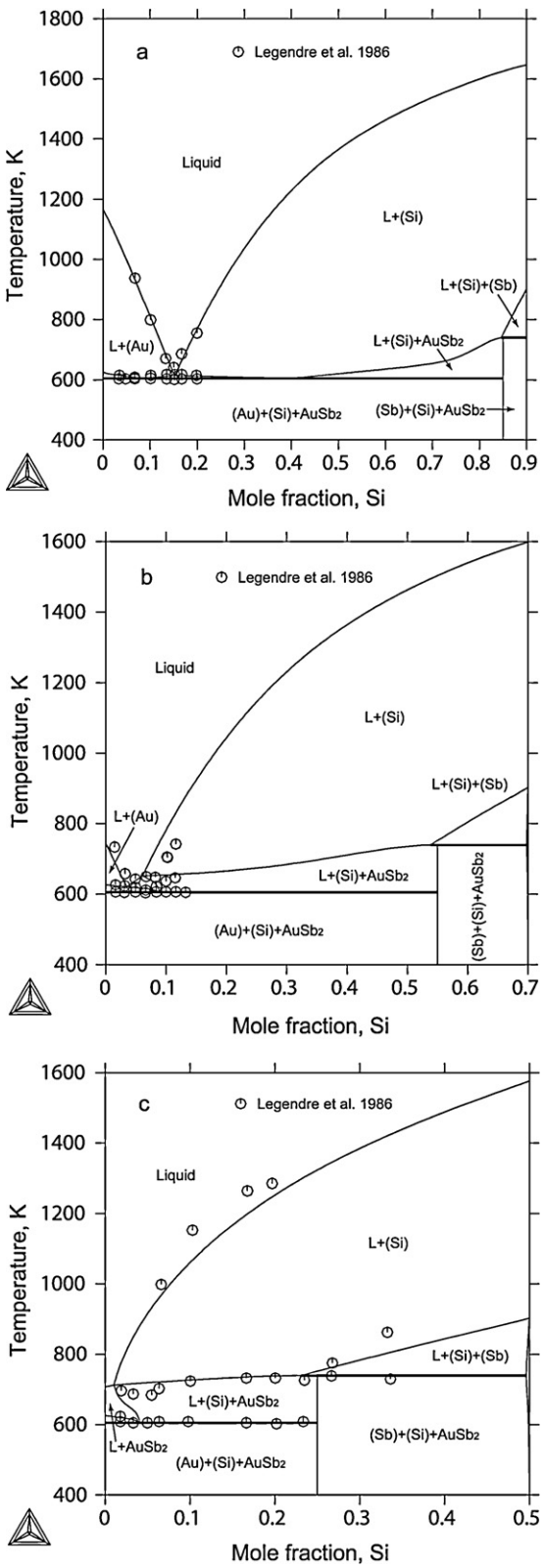

Fig. 12. Calculated vertical sections of the different Sb compositions with the experimental data [60]. (a) 10 at.% Sb; (b) 30 at.% Sb; and (c) 50 at.% Sb.

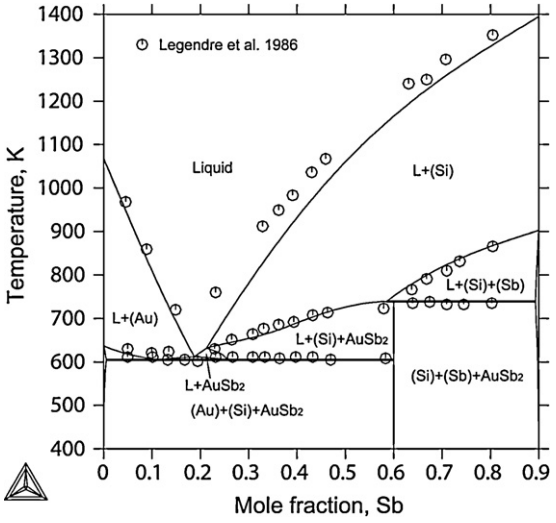

Fig. 13. Calculated vertical section at 10 at.% Si with the experimental data [60].

of fcc_A1(Au) and diamond_A4(Si) show a slight deviation from the measured experimental data [60].

6. Conclusions

The updated optimization of the Au–Sb binary system was carried out and the Sb–Si binary system was assessed using the CALPHAD method. The self-consistent thermodynamic parameters for describing various phases in these two binary systems were obtained, which can be used to reproduce well the reported experimental information. Combined with the previous assessment of the Au–Si binary system and the available experimental information on the Au–Sb–Si ternary system, thermodynamic description of the Au–Sb–Si ternary system was developed. The liquidus projection and several vertical sections were calculated. The calculated results are in good agreement with the reported experiment data.

Acknowledgements

This work was financially supported by Scientific Research Foundation for Advanced Talents in Guilin University of Electronic Technology, National Science Foundation of China (Grant Nos. 50771106, 50971136 and 50731002) and Key Project of Chinese Ministry of Education (No. 109122).

References

[1] S.K. Seo, S.K. Kang, D.Y. Shih, H.M. Lee, Microelectron. Reliab. 49 (2009) 288.
[2] V. Chidambaram, J. Hald, R. Ambat, J. Hattel, JOM 61 (6) (2009) 59.
[3] K. Suganuma, S.-J. Kim, K.-S. Kim, JOM 61 (1) (2009) 64.
[4] N. Kang, H.S. Na, S.J. Kim, C.Y. Kang, J. Alloys Compd. 467 (2009) 246.
[5] S.J. Kim, K.-S. Kim, S.-S. Kim, K. Suganuma, J. Electron. Mater. 38 (2009) 266.
[6] P. Fima, W. Gasior, A. Sypien, Z. Moser, J. Mater. Sci. 45 (2010) 4339.
[7] H. Schoeller, S. Bansal, A. Knobloch, D. Shaddock, J. Cho, J. Electron. Mater. 38 (2009) 802.
[8] J.S. Kim, W.S. Choi, D. Kim, A. Shkel, C. Lee, Mater. Sci. Eng. A 458 (2007) 101.
[9] Y.C. Liu, J.W.R. Teo, S.K. Tung, K.H. Lam, J. Alloys Compd. 448 (2008) 340.
[10] J.-W. Yoon, H.-S. Chun, S.-B. Jun, J. Alloys Compd. 469 (2009) 108.
[11] V. Chidambaram, J. Hald, J. Hattel, J. Alloys Compd. 490 (2010) 170.
[12] J. Wang, H.S. Liu, Z.P. Jin, CALPHAD 28 (2004) 91.
[13] J. Wang, H.S. Liu, L.B. Liu, Z.P. Jin, Trans. Nonferrous Met. Soc. China 17 (2007) 1405.
[14] J. Wang, H.S. Liu, L.B. Liu, Z.P. Jin, CALPHAD 31 (2007) 545.
[15] J. Wang, F.G. Meng, H.S. Liu, L.B. Liu, Z.P. Jin, J. Electron. Mater. 36 (2007) 568.
[16] J. Wang, C. Leinenbach, M. Roth, J. Alloys Compd. 481 (2009) 830.
[17] J. Wang, C. Leinenbach, M. Roth, J. Alloys Compd. 485 (2009) 577.
[18] J. Wang, C. Leinenbach, M. Roth, CALPHAD XXXVIII (2009), Prague, Czech Republic.
[19] J. Wang, F.G. Meng, M.H. Rong, L.B. Liu, Z.P. Jin, Thermochim. Acta 505 (2010) 79.
[20] H.S. Liu, C.L. Liu, C. Wang, Z.P. Jin, K. Ishida, J. Electron. Mater. 32 (2003) 81.
[21] H.S. Liu, C.L. Liu, K. Ishida, Z.P. Jin, J. Electron. Mater. 32 (2003) 1290.
[22] H.S. Liu, K. Ishida, Z.P. Jin, Y. Du, Intermetallics 11 (2003) 987.
[23] H.S. Liu, Y. Cui, K. Ishida, Z.P. Jin, CALPHAD 27 (2003) 27.
[24] H.S. Liu, J. Wang, Y. Du, Z.P. Jin, Z. Metallkd. 95 (2004) 45.
[25] F.G. Meng, H.S. Liu, L.B. Liu, Z.P. Jin, J. Alloys Compd. 431 (2007) 292.
[26] H.Q. Dong, S. Jin, L.G. Zhang, J.S. Wang, X.M. Tao, H.S. Liu, Z.P. Jin, J. Electron. Mater. 38 (2009) 2158.
[27] L. Kaufman, H. Bernstein, Computer Calculation of Phase Diagrams, Academic Press, New York, 1970.
[28] N. Saunders, A.P. Modwnik, CALPHAD-A Comprehensive Guide, Pergamon, Lausanne, Switzerland, 1998.
[29] B. Sundman, B. Jansson, J.O. Anderson, CALPHAD 9 (1985) 153.
[30] H. Okamoto, T.B. Massalski, Bull. Alloy Phase Diagrams 5 (1984) 166.
[31] P.Y. Chevalier, Thermochim. Acta 155 (1989) 211.
[32] J.H. Kim, S.W. Jeong, H.M. Lee, J. Electron. Mater. 31 (2002) 557.
[33] R.W. Olesinski, G.J. Abbaschian, Bull. Alloy Phase Diagrams 6 (1985) 445.
[34] A.T. Dinsdale, CALPHAD 15 (1991) 317.
[35] R. Vogel, Z. Anorg. Chem. 50 (1906) 145.
[36] A.T. Grigorjew, Z. Anorg. Chem. 209 (1932) 289.
[37] D.S. Evans, A. Prince, CALPHAD XIII, Villard de Lans, France, 1984.
[38] B. Gaither, R. Blachnik, Z. Metallkd. 67 (1976) 395.
[39] P.C. Wallbrecht, R. Blachnik, K.C. Mills, Thermochim. Acta 45 (1981) 189.
[40] E. Zoro, C. Servant, B. Legendre, J. Alloys Compd. 426 (2006) 193.
[41] E. Hayer, R. Castanet, Z. Metallkd. 86 (1995) 8.
[42] E.A. Owen, E.A.O. Roberts, J. Inst. Met. 71 (1945) 213.
[43] P. Anres, H. Bros, R. Castanet, Intermetallics 2 (1994) 285.
[44] K. Kameda, T. Azakami, M. Kameda, J. Jpn. Inst. Met. 38 (1974) 434.
[45] M. Hino, T. Azakami, M. Kameda, J. Jpn. Inst. Met. 39 (1975) 1175.
[46] A.K. Jena, M.B. Bever, Trans. Met. Soc. AIME 242 (1968) 1453.
[47] F. Weibke, G. Schrag, Z. Elektrochemie 46 (1940) 658.
[48] W. Biltz, G. Rohlffs, H.U. Vogel, Z. Anorg. Allg. Chem. 220 (1934) 113.
[49] O.J. Kleppa, J. Phys. Chem. 60 (1956) 858.
[50] A. Yassin, R. Castanet, High Temp. Mater. Proc. 16 (1997) 209.
[51] R.S. Williams, Z. Anorg. Chem. 55 (1907) 1.
[52] C.D. Thurmond, M. Kowalchik, Bell. Sys. Tech. J. 39 (1960) 169.
[53] B. Girault, C.R. Hebd, Séances Acad. Sci. B 248 (1977) 1.
[54] Y. Malmeja, P. Desré, E. Bonnier, Mém. Sci. Rev. Métall. 69 (1972) 565.
[55] C.S. Fuller, J.A. Ditzenberger, J. Appl. Phys. 27 (1956) 544.
[56] J.J. Rohan, N.E. Pickering, J. Kennedy, J. Electrochem. Soc. 106 (1959) 705.
[57] F.A. Trumbore, Bell. Sys. Tech. J. 39 (1960) 205.
[58] D. Nobili, R. Angelucci, A. Armigliato, E. Landi, S. Solmi, J. Electrochem. Soc. 136 (1989) 1142.
[59] A.Y. Gubenko, I.K. Kiparisova, Izv. Askad. Nauk. SSSR Neorg. Mater. 7 (1971) 1149.
[60] B. Legendre, C. Hancheng, Bull. Soc. Chim. France 2 (1986) 138.
[61] A. Prince, G.V. Raynor, D.S. Evans, Phase Diagrams of Ternary Gold Alloys, The Institute of Metals, London, 1990.
[62] G. Humpston, S.P.S. Sangha, J. Phase Equilibira 14 (1993) 659.
[63] O. Redlich, A.T. Kister, Ind. Eng. Chem. 40 (1948) 345.
[64] Y.M. Muggianu, M. Gambino, J.P. Bros, J. Chim. Phys. 72 (1975) 83.